Materials Advances

ROYAL SOCIETY OF CHEMISTRY

PAPER

View Article Online
View Journal | View Issue

Cite this: *Mater. Adv.*, 2026, 7, 3328

The effect of solvent on the functional properties of zinc oxide films *via* AACVD

Oliver R. Marsh, Iqra Ramzan, Claire J. Carmalt and Ivan P. Parkin *

Zinc oxide films were successfully synthesised from zinc acetate dihydrate in a dual-solvent mixture *via* aerosol assisted chemical vapour deposition (AACVD). Preferential growth in the (002) and (100) crystal planes was achieved through variation in the dielectric constants of the solvents. It was found that the solutions with greater dielectric constants increased the growth in the (002) direction, whilst toluene, which has a low dielectric constant, increased growth in the (100) plane. This leads to the ability to grow functional zinc oxide films with specific morphologies for a range of PV devices to optimise electron transport. Excellent conductivities of ~6 and 1.3 S cm^{-1} were obtained for undoped zinc oxide, using acetonitrile and toluene as the secondary solvents respectively, demonstrating that the morphology has little influence on Hall effect measurements. All films were transparent, where some met industry standards, reaching over 80% transmittance to visible light. Highly crystalline films have been produced, with low FWHM confirmed by XRD analysis, making these films suitable for doping to enhance their functionalities as electron transport layers. Water contact angle measurements confirmed the presence of both hydrophobic and hydrophilic zinc oxide films. The origin of the differing surface wettability was attributed to varying amounts of surface hydroxyl terminations, as determined by XPS analysis, demonstrating that the choice of solvent in the AACVD process can modify the ZnO surface chemistry and optimise for antisoiling purposes.

Received 4th August 2025,
Accepted 10th February 2026

DOI: 10.1039/d5ma00850f

rsc.li/materials-advances

Introduction

With solar power set to be the predominant source of energy world-wide by the mid-2030s, the need for more efficient photovoltaics (PVs) is higher than ever. The photocurrent efficiency (PCE) of some commercially available PVs has reached 26.7% for c-Si, 22.9% for CIGS ($Cu(In,Ga)Se_2$), and 22% for CdTe solar cells.[1–3] The improvement in PCE has partly come from the incorporation of interface layers between photon absorption layers and the transparent conducting oxide (TCO) or encapsulant layers which reduce charge recombination. One interface material of interest is zinc oxide, a highly crystalline semiconductor where its wide band-gap (3.37 eV) lends itself to having high transparency.[4]

Aerosol assisted chemical vapour deposition (AACVD) is a method used to deposit thin films which has some major benefits over its predecessor (atmospheric pressure (AP) CVD). APCVD relies on the volatility of the precursors, whereas AACVD only relies on the solubility of a precursor in a chosen solvent.[5] Therefore, this opens the possibilities as to what precursors are available for film deposition, with non-volatile precursors now able to be deposited by AACVD. The choice of solvent is influential in the characteristics of the film grown, where morphology, phase structures, transparency, conductivity, and grain sizes can all be affected.[6,7] Zinc oxide can be deposited *via* AACVD from a zinc acetate precursor that is soluble in a range of solvent systems, each giving different film properties.

During AACVD, a precursor is dissolved in solvent and then transformed into a mist using an ultrasonic nebuliser. This aerosol mist is then carried to the deposition chamber in an inert gas stream. The mist is heated to temperatures typically ranging from 300 to 550 °C, where the solvent evaporates, leaving the precursor to deposit onto the substrate. Using different solvents affects the kinetics of this process, with higher viscosity solutions producing larger droplets which takes more time to completely evaporate.[8,9] Thus, it is expected that higher viscosity, and higher boiling point solutions will cause greater levels of carbon incorporation into the films. Different solvents also cause different reactive intermediates to form, which react homogenously onto the substrates' surface, affecting film properties.[10]

Methanol is a commonly used solvent since its high polarity allows for the high solubility of zinc acetate. Although non-polar solvents such as hexane and toluene don't have the ability to dissolve zinc acetate, they can be utilised when incorporated into mixtures with high methanol mole fractions. For a MeOH:*n*-hexane solution where it's mole fraction is 0.865, a micellar regime occurs, where methanol makes up the hydrophilic outer-core, and hexane the hydrophobic inner-core.[11] Zinc acetate interacts strongly with the methanol molecules

Department of Chemistry, University College London, 20 Gordon Street, London WC1H 0AJ, UK. E-mail: i.p.parkin@ucl.ac.uk

in the outer core, hence why the dissolution takes place with no phase separation.

The nature of zinc oxide interfaces can be tuned for different PV technologies, depending on the surface roughness and conduction band of the photon absorber which has been deposited onto it. Smooth surfaces have been shown to increase adhesion with the absorber layer, whereas rougher surfaces improve light scattering. Hence, tuning the surface roughness of ZnO would be a powerful way to optimise electron transport across the film interface, increasing PCE.[6] Another consideration is the band alignment at the boundary between the interface layer and the photo absorber. Sanchez-Perez *et al.* has demonstrated that the solvent mixture can significantly alter the band-gap of the zinc oxide film using $Zn(acac)_2$ as the precursor.[12] Optimising the band-gap improves electron transfer by ensuring that the barrier for charge extraction is not too high or low. Hydrophobic and hydrophilic surfaces are becoming increasingly attractive for antisoiling purposes. The degree of wettability can be controlled by surface modifications, the surface free energy and surface roughness of the films. Some previous literature outlines routes to achieving various degrees of wettability, using materials such as *n*-octadecyl thiol, polyethylene terephthalate, and poly-vinyl alcohol.[13–15] Whilst these reports have all been greatly successful, they require additional synthesis steps which can often be time consuming and expensive. In this study, we have found that the solvent affects the surface chemistry of zinc oxide films, changing their wettability. This has led to a facile route for surface modifications to improve the films antisoiling properties. To our knowledge, this is the first time that the dielectric constant of the solvent and the texture coefficient of the (002) plane have been related, allowing for control of the film's orientation. This paper also provides an in-depth discussion of how a dual solvent mixture affects the physical properties of zinc oxide films such as carrier mobility, morphology and transmittance of visible light, which can further be optimised for the films' use as interfacial layers in solar cell design.

Experimental

All AACVD depositions were carried out using nitrogen (99.99%, BOC, Surrey, UK) as the carrier gas, with a flow rate of 1 L min^{-1}. Zinc acetate dihydrate (0.5 g, 2.28 mmol) was the precursor of choice, purchased from Alfa Aesar, and no purification was required. A precursor solution was made up in a thinned out round bottom flask, where zinc acetate dihydrate was dissolved in 30 mL of solvents (Table 1). Acetic acid ($\sim$1 mL) was added to all solutions to aid solubility; the flask was then mixed ultrasonically for 15 minutes each. The glass substrates that are to be deposited on were 3.2 mm thick barrier glass (Pilkington Technology Management Limited, Lancashire, UK). These were cleaned ultrasonically using a methanol and acetone solution, then were dried in an oven prior to deposition.

Before misting, the glass substrate was placed on top of a carbon block inside the AACVD apparatus (Fig. 1) which was subsequently heated to 450 °C. A top plate was also preloaded which sat vertically 8 mm above the substrate to ensure laminar flow. Once the temperature was reached, the solution was deposited onto the substrate as a mist. The mist was generated by a 1.6 MHz piezo ultrasonic atomiser (Johnson Matthey) and transferred to the AACVD rig *via* a nitrogen carrier gas. After all reactions went to completion, the apparatus was cooled at 10 °C min^{-1} under nitrogen gas, to yield zinc oxide films.

Table 1 Solvent systems used for each deposition. The boiling point, viscosity, and dielectric constant data are representative of solvent 2

Solvent 1 (20 mL)	Solvent 2 (10 mL)	Boiling point (°C)	Viscosity (cp, 20 °C)	Dielectric constant (20 °C)
Methanol	Methanol	64.7	0.55	32.6
Methanol	Toluene	110.6	0.59	2.4
Methanol	Ethyl acetate	77.0	0.46	6.02
Methanol	*n*-Hexane	69.0	0.31	1.89
Methanol	Tetrahydrofuran (THF)	66.0	0.55	7.6
Methanol	Acetonitrile	82.0	0.37	37.5

Characterisation

Scanning electron microscope images were taken using a JEOL JSM-7600F at an acceleration voltage of 10.0 kV. Film thicknesses were calculated by averaging the thickness across the substrate at three separate locations from side-on images. X-ray diffraction patterns were recorded using a Malvern Panalytical Empyrean X-ray diffractometer, which used monochromatic $CuK\alpha_1$ and $k\alpha_2$ radiation wavelengths of 1.54056 and 1.54439 Å respectively. These wavelengths were emitted at an intensity of 2 : 1 with a voltage of 40 kV and a current of 40 mA. Data were collected for 2θ angles of 10–80° at 0.05° intervals, each taking 0.5 seconds per interval. FWHM was found using data collector software powered by Malvern Panalytical. UV-Vis spectroscopy was conducted using a Shimadzu 3600i plus spectrometer over a range of 200–3000 nm. Hall measurement data were collected using an Ecopia SPCB-01 set-up, where resistivity, conductivity, and carrier mobility data were found using a $\sim$1 cm^2 substrate. One dimensional ^1H NMR spectra were collected using a Bruker Avance Neo 500 and analysed using MestReNova software. Water droplet surface contact angles were measured using a

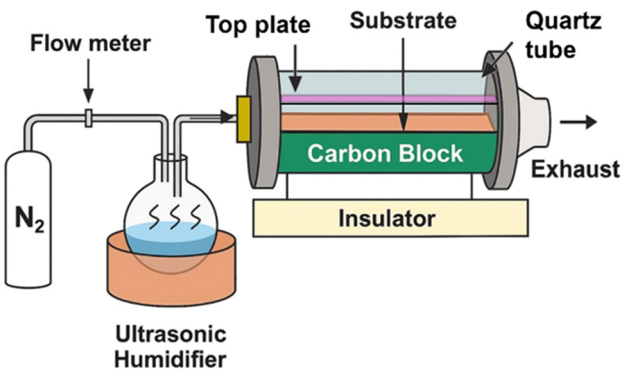

Fig. 1 AACVD apparatus.

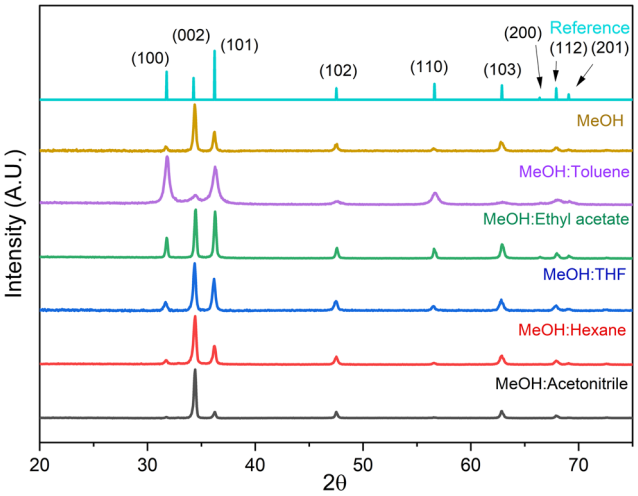

Fig. 2 XRD patterns of zinc oxide films grown using different solvent mixtures. The reference data is of hexagonal wurtzite (JCPDS no. 00-036-1451). The peaks observed at 31.76, 34.41, 36.25, 47.53, 56.59, 62.85, 67.94, and 69.09 correspond to the (100), (002), (101), (102), (110), (103), (112), and (201) respectively.[18]

Krüss DSA25E drop shape analyser and subsequently analysed using Krüss Advance software. Transmittance and reflectance data were collected on a Shimadzu UV-3600i plus. X-ray photoelectron spectroscopy (XPS) was conducted on a Thermo K-alpha X-ray photoelectron spectrometer, and analysed using Avantage software.

Results and discussion

The solvent used during AACVD was found to have a large impact on the morphology and optoelectronic properties of ZnO thin films. During this process a dual-solvent mixture was atomised using an ultrasonic humidifier. Despite all solvent being transferred to the reactor, some residue of zinc acetate was left behind in all cases. High quality films were produced throughout, passing the Scotch tape™ test showing good adhesion, high transparency, and the ability for reproducible results.

The coordination chemistry in the solution phase of the zinc precursor was studied by ^{1}H NMR. This indicated that there was no direct evidence for the existence of methanol, or any other secondary solvents coordinating to zinc acetate (Fig. S1–S13). One observation was the peak broadening of the singlet at 0.94 ppm, compared to other solvent mixtures. This was indicative of an OH group, when a methanol:*n*-hexane mixture was used. Peak broadening can explain micellar formation mentioned previously, as a broader peak shows a dynamic hydrogen bonding network.[16] However, NMR studies were not conclusive in realising the coordination chemistry of zinc acetate in various solvents, and the changes in these structures in the gas phase are widely unknown.

X-ray diffraction (XRD) patterns provide information regarding the crystallinity, orientation, and crystallite sizes for the films produced. Fig. 2 shows XRD patterns for the films grown using different solvent mixtures. The solvent system used affects the crystallinity of the films as observed by the full width half maxima (FWHM) of the (002) crystal planes (Table 2). Since the variable was the solvent mixture, the difference in crystallinity of the films must be due to the solvents physical and chemical properties such as the boiling point, viscosity, and dielectric constant. A low boiling point, low viscosity, and high dielectric constant are ideal requirements for a good precursor mixture due to the ease of droplet formation (dielectric constant), and the ease of evaporation (low boiling point, low viscosity).

XRD data reveal that a mixture of MeOH:acetonitrile has the smallest FWHM, indicating high crystallinity (Fig. 2). This is because this solvent mixture has the highest dielectric constant with low viscosities, meaning that smaller droplets form.[17] Using methanol only also gives similar results, however they are not as extreme, as its viscosity and dielectric constant are lower than acetonitrile. Despite MeOH:*n*-hexane films having no phase separation, this was the only mixture in which zinc acetate did not fully dissolve, and a solution with a pale white colour was observed. However, good quality films were still achieved with XRD showing high crystallinity, and a similar preference for growth as with just methanol.

The crystallite diameters were calculated using the Scherrer equation:[7]

$$D = \frac{k\lambda}{\beta \cos\theta}$$

D is the average size of the crystals, k is a dimensionless shape factor which has been taken as 0.9 in this instance, λ is the wavelength of the incident X-rays, β is the FWHM in radians, and θ is the Bragg diffraction angle in radians.

Table 2 Crystal data regarding the six solvent mixtures investigated. The texture coefficient and FWHM are that of the (002) crystal plane. The relative intensity of the peaks is calculated by dividing the normalised (002) and (100) peaks by each other. The relative intensity for the reference (JCPDS no. 00-036-1451) is 0.77. The errors for film thickness are in brackets within the table

Solvent	Texture coefficient (002)	FWHM (002) (+/− 0.0083)	Relative intensity of (002) against the (100) peak	Crystallite diameter/nm (+/− 0.9 nm)	Film thickness (nm)
MeOH	3.86	0.261	7.45	31.9	313 (±36)
MeOH + toluene	0.73	0.469	0.20	17.0	390 (±25)
MeOH + ethyl acetate	2.64	0.234	2.39	34.1	498 (±32)
MeOH + *n*-hexane	3.89	0.297	10.98	28.0	670 (±56)
MeOH + THF	3.22	0.275	5.00	30.2	435 (±83)
MeOH + acetonitrile	4.72	0.232	40.00	35.9	428 (±61)

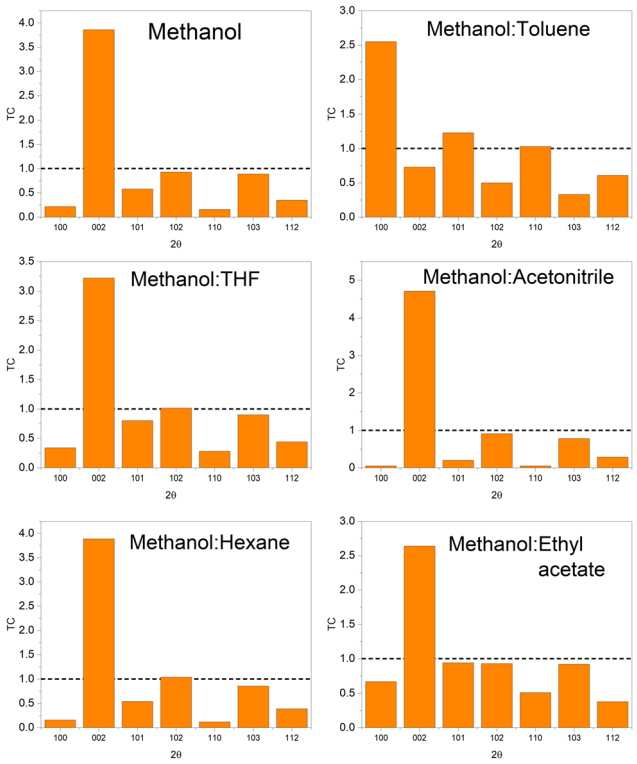

Fig. 3 Texture coefficient data compared to a standard from the National Institute of Standards and Technology (NIST). The red dotted horizontal line indicates a texture coefficient of 1, deviation from this line shows a preference for orientation.

Despite XRD data showing that the films have different intensities in different crystal planes, when compared to a standard powder sample it is apparent that ZnO films deposited *via* the AACVD process naturally prefer growth in the (002) plane.[18] This is shown in Fig. 3, where a texture coefficient was calculated using the following equation:

$$\text{Texture coefficient } (hkl) = \frac{I(hkl)/I_0(hkl)}{\frac{1}{N}\sum_N I(hkl)/I_0(hkl)}$$

where I is the measured intensity, I_0 is the intensity if the standard is used, and N is the number of reflections. Note that if the film had the same orientation as the standard, all the peaks would be at a value of 1. The texture coefficient is a way to quantify how great the propensity is for crystal growth in a particular direction compared to a reference, and this is known as preferential orientation.

In the XRD data (Fig. 2), the (101) peak is more intense than the (002) for the toluene mixture and is very similar to when using ethyl acetate. In these instances, the (100) plane has become more prominent, due to being geometrically linked by the *a* axis. By the same reasoning, the (101) and (002) must also be related by the *c* axis, hence, to remove this inherent correlation, the relative intensities of (002) against the (100) plane were calculated and are shown in Table 2. In Fig. S14, the texture coefficient and the ratio of the (002)/(100) planes are shown to be related by an exponential curve model. The tendency for preferred growth in the (002) plane is therefore very sensitive to the dielectric constant of the solvent mixture. It is also weakly correlated to the structure factor, since an exponential model best fits the data instead of a linear one.

All the solvent mixtures have at least two thirds of the solvent mixture containing methanol, the most polar of all organic solvents. This is significant when understanding the layering of hexagonal zinc oxide, where Zn and O atoms stack alternatively along the *c*-axis creating a polar crystal structure.[19] Therefore, it is expected that a droplet containing the solution of the highest dielectric constant will have the strongest interactions with the *c*-axis on the substrate, causing the high degree of self-texturing observed.[20] The texture coefficient for the (002) plane increases as the dielectric constant of the solvent mixture increases, indicating that control over the films' preferential orientation can be achieved by choice of solvent. Using toluene as the secondary solvent produced ZnO films with little preference in the (002) plane. Toluene, being the least polar solvent, meant that there was a much greater influence for growth in the non-polar (100) and (101) directions, showing the sensitivity to solvent in the AACVD process. These observations are consistent with Sanchez *et al.*, who reported similar preferential orientation using methanol:toluene mixtures when using diethyl zinc as the precursor.[21] The only exception to this trend was the mixture comprised of methanol and hexane. The preference for growth is understood to be due to zinc acetate interacting with just methanol molecules, since hexane is the least polar solvent, and hence will have the weakest attractions to the precursor. There is a moderate relationship between the dielectric constant of the secondary solvent and the texture coefficient as it has a regression value of 0.71 (Fig. S15). Due to preferential orientation being controlled by the solvent mixture, this process has been shown to be reproducible, where when the same solvent is used, the same preference for growth was observed.

AACVD is just one of many techniques that are available for thin-film synthesis. The texture coefficients calculated show preferred growth in the (002) direction, which is directed by the polar interactions of methanol and zinc acetate with the polar *c*-axis. Spin-coating has been shown to result in low preference for deposition in the *c*-axis. Sunaina *et al.* used a mixture of ethanol and ethylene glycol *via* thermal decomposition of zinc acetate dihydrate at 300 °C, where zinc oxide films showed the greatest preference in the (100), (101), and (110) crystal planes.[22] Kamaruddin *et al.* used a sol–gel method with zinc acetate dihydrate and isopropanol, where the dominant peaks were (100) and (101), and the (002) plane was present at roughly half the intensity.[23] Plasma-assisted mist CVD (PAMCVD), reported by Takenaka *et al.* showed the preference of (002) from a solution of ethanol and zinc acetate in a O_2/Ar plasma.[24] Using APCVD can also form zinc oxide nanostructures with preference for the (002) plane, from zinc acetate dissolved in water.[25] Spin-coating and PAMCVD use a similar solvent system, but the reason for contrasting orientations is due to the methodology itself, where gas phase and liquid phase

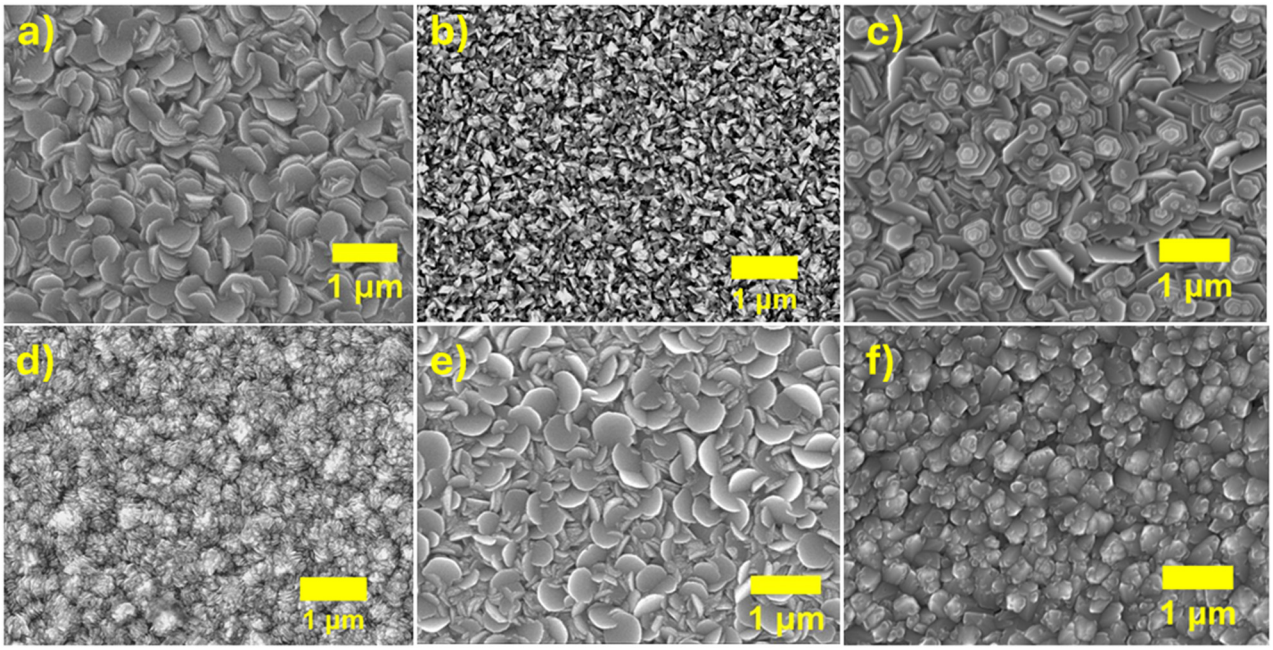

Fig. 4 SEM pictures at 20 000× magnification (a) MeOH, (b) MeOH:toluene, (c) MeOH:hexane, (d) MeOH:ethyl acetate, (e) MeOH:THF, and (f) MeOH:acetonitrile. Each scale bar is 1 μm in length.

chemistry produce different reactive species for deposition. AACVD produces films with dominant crystal planes in the (002), (100), and (101) directions due to different reactive species forming in the gas phase from the solvent system used.

Scanning electron microscope (SEM) images provide a detailed picture of the surface morphology of thin-films. There is a difference in grain sizes across the films (Fig. 4), and the discrepancy in the crystallite sizes calculated is mentioned in the previous section. Larger grains are formed by films having lower surface energies and lower preference for orientation, causing coalescence of smaller crystallites into larger grains.[26] In Fig. 4, zinc oxide films display a range of morphologies that are a direct consequence of the use of different solvent systems. When methanol, hexane, and THF are used, hexagonal discs form (**4a**, **4c**, **4e**). The film grown using ethyl acetate (**4d**) is also formed by hexagonal discs but the grains are randomly orientated, with many laying on their side rather than flat. A low preference for orientation, shown by the texture coefficients lying between 0.5 and 2.5, causes the morphology to become less ordered, hence the lack of distinct grains. Fig. 4c differs from other hexagonal structures, in this case there is a high degree of stacking, with nucleation sites at the centre of the hexagons. Zinc oxide grown using methanol and toluene (**4b**) forms films with small, triangular shaped grains which is exemplified by its preferential growth in the (100) plane, and its high FWHM in the (002) plane (Table 2). Methanol and acetonitrile films form pyramid-like structures which have a high desire for growth in the (002) direction. The addition of a secondary solvent that is less polar than methanol shows less preference for growth along the (002) plane, until another plane becomes more dominant, such as when using toluene. Since all mixtures are miscible, zinc acetate is able to fully dissolve, and can therefore interact with solvents less polar than methanol, in which case the preference for growth in the (101) and (100) non-polar planes increases.[27] This has a roughening effect on the films due to more irregularly shaped grains, as shown in the side-on SEM images inFig. 5. For electron transport layer (ETL) applications smoother surfaces have shown to result in higher PCEs due to the greater surface contact between the grains.[28]

The hexagonal discs shown are common to zinc oxide films grown *via* AACVD.[29] Hexagonal grains are able to be synthesised by other methods such as solution phase synthesis, and spin coating.[30] Different morphologies have been observed when using other techniques, such as spray pyrolysis where rod-like and spherical-shaped grains are grown, even though the XRD pattern reveals a dominance in the (002) plane.[31] Dip coating has been shown to produce films that are granular and rod-like, and nanorods can be formed *via* thermal evaporation.[22,32] The choice of precursor, solvent, and deposition technique is crucial in dictating the morphology, and the preferential growth in zinc oxide thin films. In these experiments, we show that the morphology is able to be dictated by changing only the solvent used, leading to a facile and selective route for a range of zinc oxide thin films.

Side-on SEM images (Fig. 5) provide information with regard to the surface roughness of the films. The thickness varies across the films (Table 2), and the images have been taken in different areas across each substrate, where the conductivity was found to be the greatest. This was due to high conductivity being the selection criteria for analysis, since our focus was on the TCO properties of zinc oxide. Another reason for thickness variation across the substrate was due to the droplet nucleation rates, as they differ with the solvent system. In the case of methanol:hexane, the area of film with the highest conductivity was found

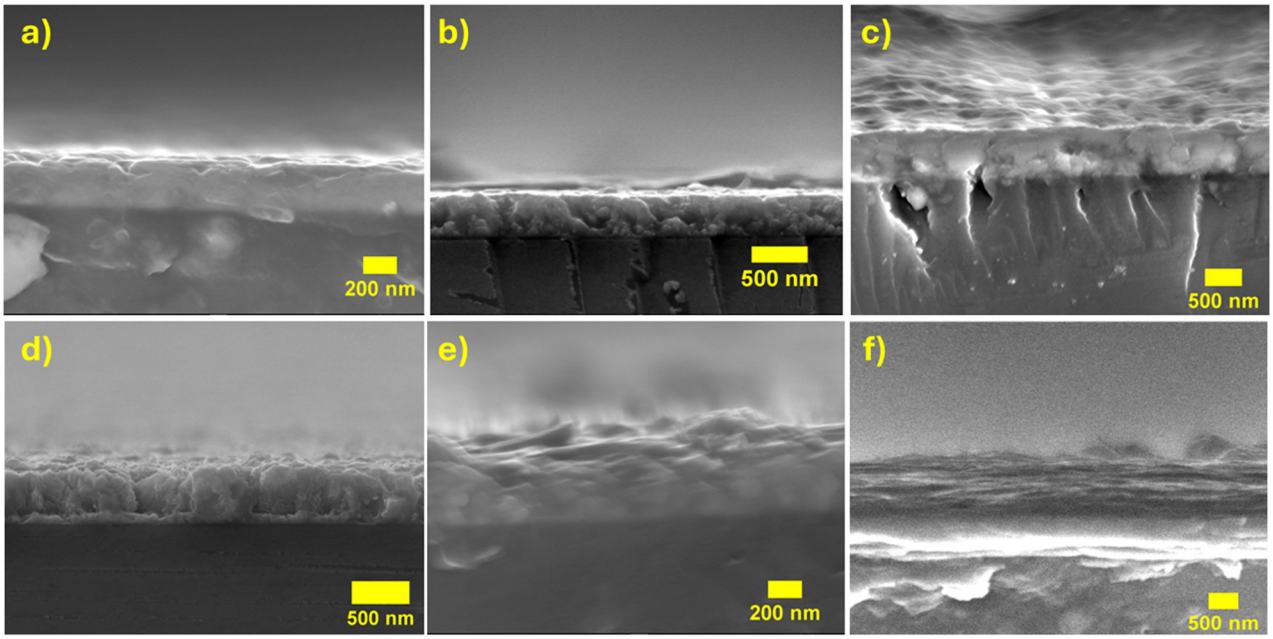

Fig. 5 Side-on SEM images: (a) MeOH, (b) MeOH:toluene, (c) MeOH:hexane, (d) MeOH:ethyl acetate, (e) MeOH:THF, and (f) MeOH:acetonitrile.

towards the end of the substrate, whereas for the other solvents, the area of interest was somewhere in the middle.

The electronic properties for zinc oxide are commonly related to the film thickness, grain overlap and uniformity, as well as the amount of oxygen vacancies, V_O across the crystal structure. Films deposited using acetonitrile and toluene as the secondary solvents show high conductivities of 6.13 and 1.3 S cm^{-1} respectively. The preferential growth in different crystal planes provides evidence that the orientation and morphology of zinc oxide can be selected, with little sacrifice to its electronic properties. THF has very low conductivity; its apparent high roughness, which can be gauged from the error in thickness calculation, increases electron scattering at the grain boundaries.[33] The carrier concentration is five to seven orders of magnitude lower than the other solvent systems, thus reducing the number of electrons that percolate through the grains.

Standard AACVD procedures for zinc oxide films from zinc acetate using only methanol as the solvent.[34,35] When one third acetonitrile is added, the conductivity and mobility both increase by 50 times to 6.13 S cm^{-1} and to 2.00 cm^2 V^{-1} s^{-1} respectively (Table 3). This follows the following equation by which the carrier concentration, conductivity, and mobility are related by:

$$\sigma = qn\mu$$

where σ is the conductivity, q is the elementary charge, n is the carrier concentration, and μ is the mobility.[36] Despite films using methanol and acetonitrile having the same carrier concentrations, the improvement of the electron mobility is due to changes in surface morphology from hexagonal platelets to truncated pyramids, and the increase in preference for the (002) plane (Fig. 6).[37,38] It is deduced that the mobility and carrier concentration are inversely related to each other, and indeed that is what the experimental data show in Fig. 6, with a high regression value of 0.98. As all films were deposited on highly resistive barrier glass, substrate contributions to the conductivity can be ruled out, and were not subtracted in the calculations.

Transparent films were grown across all solvent mixtures exhibiting transmittances between 56 and 80% (Table 4). The transmittance values differ between solvent mixtures used, likely due to varying degrees of residual carbon incorporated into the films. Adventitious carbon was found to be present on all films (Fig. S16), where the main C 1s peak was charged referenced to 284.8 eV. Oxygen XPS also showed the presence of some O–C species at ~533.0 eV (Fig. 9). Although etching wasn't conducted to provide depth scans, it is well understood that the decomposition of the zinc acetate causes carbon to be incorporated into the lattice structure of the films.[39] The SEM

Table 3 Electronic properties of zinc oxide films grown using different solvent systems

Solvent	Conductivity (S cm^{-1})	Resistivity (Ω cm)	Mobility (cm^2 V^{-1} s^{-1})	Carrier concentration (cm^{-3})
MeOH	0.120	8.35	0.040	1.89×10^{19}
MeOH:toluene	1.300	0.77	3.65	2.22×10^{18}
MeOH:ethyl acetate	0.180	5.57	11.10	1.01×10^{17}
MeOH:hexane	0.614	1.63	1.28	3.00×10^{18}
MeOH:THF	1.47×10^{-4}	6800	26.7	3.51×10^{12}
MeOH:acetonitrile	6.130	0.16	2.00	1.89×10^{19}

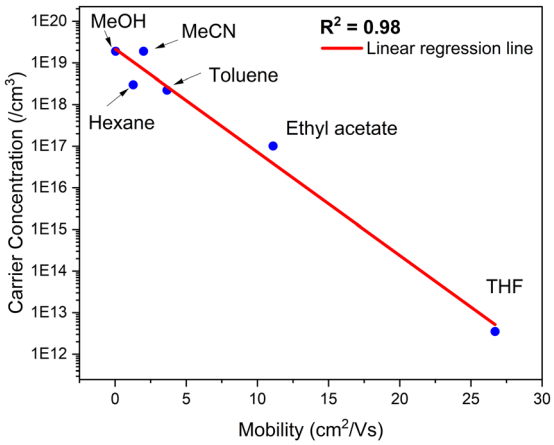

Fig. 6 The mobility values have been plotted against the carrier concentration, and a linear regression analysis was undertaken. An R^2 value of 0.98 shows a very high correlation and highlights the reliability of the Hall data measured.

images (Fig. 4) are all homogenous, so the presence of carbon nanoclusters is unlikely. All films were found to be air stable after 5 months, where the transmittance values were all within ~2%. Only methanol showed a diminished transmittance to visible light which could indicate that some surface reactions occurred with air over time. However, this may not be the case and could be due to the positioning of the sample in the UV-vis apparatus, since all other films showed much smaller deviation from when initially tested.

The films varied in thickness (313–625 nm) depending on the solvent system used. The film density could be a factor as to why there is such variation in film thickness, but no testing was conducted to investigate this. Research groups such as Smith *et al.* have used X-ray fluorescence and ellipsometry in conjunction with SEM, where zinc oxide films with lower preferential orientation in the *c*-axis had greater film densities.[40] Moreover, the surface energy and tension of the solvents used affects the rate at which droplets evaporate, where larger ones are more likely to be lost through the exhaust. Thus, there will be a thickness gradient across the substrate, where the amount of film deposited will vary across the choice of solvents. Thicker films tend to be more opaque, whereas thinner films have shown to have higher transparencies.[41] For this study, the layer thickness was not a control, and so optical testing was merely done to show that these zinc oxide films are transparent and can become more transparent at lower film thicknesses. Industry standard fluorine doped tin oxide glass shows transmittances between 79 and 91%, and the films deposited in this study are nearing, or meet these standards.[42] ZnO films have been used as interface layers to transport electrons away from the solar layer to reduce charge recombination.[43] These film thicknesses range from 20 to 190 nm, so if the zinc oxide films produced were to be utilised as interface layers the transparency will improve as thinner films are required.

The UV-vis spectra show curves exhibiting a wave-like nature (Fig. S17), which is from the variation in thickness across the films. It is hard to achieve perfect uniformity using AACVD in small scale static reactors, and so deviation of film properties across the surface is observed. Those solvent systems which have high surface tensions and boiling points are more likely to contaminate the film with carbon.[44] However, despite toluene having the highest boiling point, the transmittance is still reasonably high at 73.2%.

Physical and chemical methods for the deposition of zinc oxide are well documented in the literature and have been summarised in Fig. 7. Whilst direct current (DC) magnetron sputtering has been found to produce films of the highest conductivities, exceeding 350 S cm^{-1}, its pitfall is the cost and scalability of the technique. Out of the others, ultrasonic spray and hydrothermal methods are just below the conductivities achieved using acetonitrile in this study, making AACVD a great choice for an industrial technique. Other methods show high transmittance of visible light, but exhibit low conductivities, which are essential for TCO materials.

Self-cleaning glass is imperative to maintain high solar absorption in PV modules due to build-up of dust particles. Hydrophobic and superhydrophobic films allow water molecules to effectively roll off their surface, picking up dirt in the process. They have water contact angles (WCA) $\geq 90^\circ$ and $\geq 150^\circ$ respectively, which stems from possessing low surface

Table 4 Transmittance and reflectance data for zinc oxide thin films grown using different solvent systems. The values used were taken at 550 nm

Solvent	Transmittance (%) (550 nm)	Reflectivity (%) (550 nm)
MeOH	80.3	9.6
MeOH:toluene	73.2	15.4
MeOH:ethyl acetate	77.0	11.7
MeOH:hexane	56.6	11.3
MeOH:THF	76.2	11
MeOH:acetonitrile	58.5	9.2

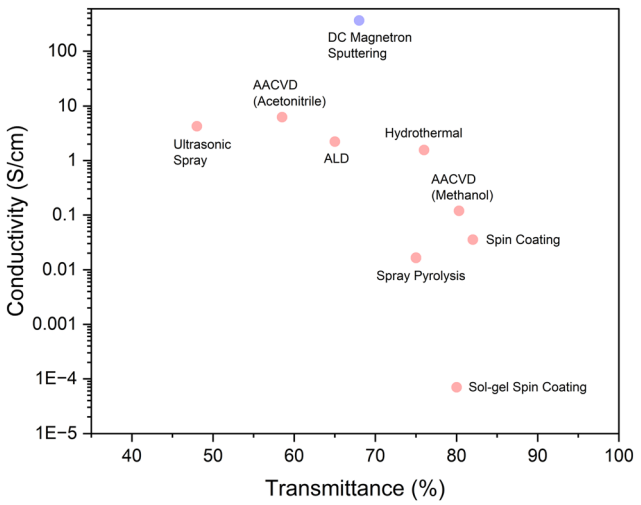

Fig. 7 A Ragone plot showing literature data for the conductivities and transmittance of zinc oxide thin films.[31,45–50] The red dots show chemical routes, and the blue dot shows a physical route for thin film deposition.

Table 5 The WCA measurements of a 5 μL water droplet on ZnO films grown using various solvent mixtures. The associated error for each WCA measurement is shown. The O–Zn/O–H ratios are calculated *via* dividing the respective peak areas from the XPS fits

Solvent	Water contact angle (°)	Error (+/− °)	O–Zn/O–H ratio
MeOH	106.3	1.96	2.19
MeOH:toluene	92.83	1.41	0.57
MeOH:ethyl acetate	91.46	2.67	0.60
MeOH:THF	107.4	4.32	1.41
MeOH:hexane	80.9	9.61	0.64
MeOH:acetonitrile	81.6	2.69	1.65

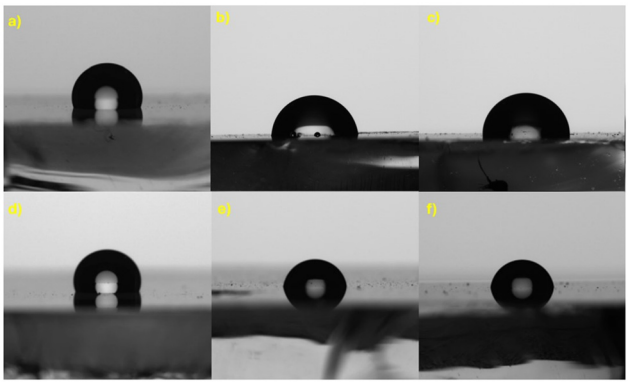

Fig. 8 5 μL water droplets on ZnO films. (a) MeOH, (b) MeOH:toluene, (c) MeOH:ethyl acetate, (d) MeOH:THF, (e) MeOH:hexane, and (f) MeOH:acetonitrile.

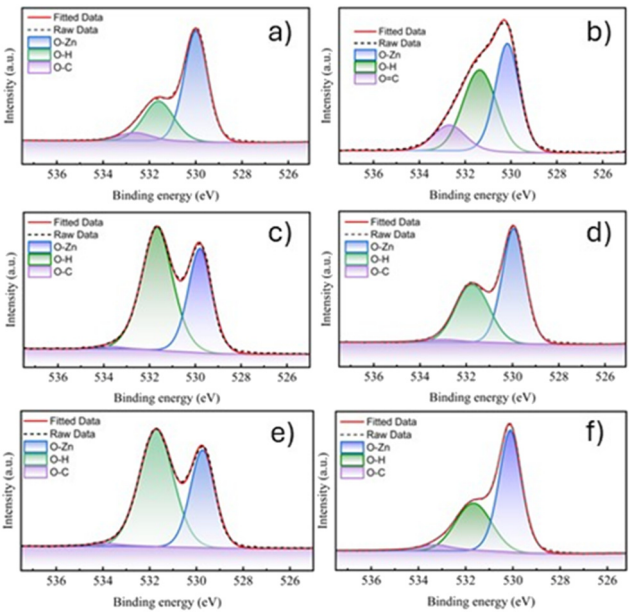

Fig. 9 XPS spectra of the oxygen 1S region, showing the presence of O–Zn, O–H, and O–C species on the surface of zinc oxide. (a) Methanol, (b) methanol:toluene, (c) methanol:hexane, (d) methanol:THF, (e) methanol:ethyl acetate, and (f) methanol:acetonitrile.

energy and high roughness.[14,51] Whereas hydrophilic and superhydrophilic coated surfaces have WCA $\leq 90^\circ$ and $\leq 10^\circ$ respectively. The mechanism of action is that water droplets wet the surface, forming a thin water film, where light can then pass through to the PV cell.

Zinc oxide is a non-toxic, transparent, and biocompatible material which makes it suitable for commercial self-cleaning glass. The superhydrophobic ZnO film has been synthesised on steel substrates with a WCA of 158°, where the microstructures trap air creating a liquid-air-solid interface.[52] Conversely, superhydrophilic ZnO films grown on glass *via* a hydrothermal process show highly porous microspheres.[51] These structures show high surface roughness increasing the wettability of the surface, thereby adhering to the Wenzel model.

WCA measurements were conducted to see if the films were hydrophilic or hydrophobic in nature. Five water droplets were placed on each film, where an average value was calculated as shown in Table 5, and its associated error was found to arise from the variation of wettability across the film's surface. The median measurement was chosen to be presented in Fig. 8, where images of the water droplets on the ZnO surfaces are displayed.

The origins of the hydrophobicity can be from changes in the amount of hydroxyl terminations on the zinc oxide surface.[53,54] Other reasons such as surface roughness and energetics were not investigated in this report.[55,56] X-ray photoelectron spectroscopy was used to probe the surface makeup of the films, high-resolution scans of the oxygen region are shown in Fig. 9, and the relative hydroxyl concentrations are found in Table 5, with the peak positions and FWHM data provided in Fig. S18.

Surface modifications can be engineered through solvent choice and provide a facile route to forming moderately hydrophobic and hydrophilic films. In the O 1s XPS spectrum of the ethyl acetate film, the Zn–O region is at 529.74 eV and the O–H region is at 531.72 eV, which agrees well with previous literature.[57,58] A high surface concentration of hydroxyls is known to increase hydrophilicity by promoting water adsorption.[53,55,59] Using THF as the co-solvent shows the highest WCA, its surface is made up of a significant proportion of Zn–O terminations, and a small proportion of hydroxyl terminated species, hence it's hydrophobic nature. Using hexane as the co-solvent yielded the most hydrophilic films, where it contained the highest proportion of hydroxyl terminations.

The XPS results provide some insight into the origins for the changes in wettability across the films studied. There is some agreement that the amount of surface hydroxyls and hydrophilicity are sufficiently related. Other surface properties including surface free energy, and roughness can also contribute to varying degrees of wettability. This could explain the relatively low WCA of 81.6° in acetonitrile despite it having a greater proportion of Zn-O to OH species at the surface.

In this study, only a 2 : 1 ratio of methanol to secondary solvent was reported in detail, with a full analysis of the film's features being presented. However, using a 2 : 1 ratio of secondary solvent to methanol was investigated to see how preferential orientation changes with different solvent ratios. A common theme with using one part methanol, is the poor solubility of zinc acetate. Despite solutions showing poor

mixing, some were aerosolised and formed thin films with interesting morphologies, further showing the sole effect that solvent has on the preferred orientation of the crystal planes.

The hexane : methanol solution was the only 2 : 1 mix that could not form any film due to phase separations inhibiting aerosolization. Ethyl acetate and methanol films show a diverse range of crystal sizes (Fig. 10) which are triangular in shape. The influence of an increase in the amount of ethyl acetate compared to methanol is obvious when looking at the texture coefficients, where a decrease in preference for the (002) plane is met by an increase in (100) and (101) growth. The addition of more ethyl acetate to solution lowers the overall dielectric constant of the solution, and this is also concordant with the data for THF. This adds further evidence for the influence of the polarity of the solvent mixture during deposition. During deposition, the zinc acetate is influenced by its surrounding solvent molecules whether they are coordinating or not. The attractive forces of zinc acetate and its close environment interact strongly with either the polar (002), or the non-polar (101) and (001) planes. Toluene being the least polar solvent shows the most extreme difference in (002) crystal growth when its concentration is increased. Its morphology is very irregular, with deformed circular crystals, as well as triangular ones.

Acetonitrile has a higher dielectric constant than methanol and so based on previous data it should be expected that increasing the acetonitrile concentration increases the preference for (002) growth. In fact, a lesser observed semipolar (103) plane arises.[60] Its been hypothesised that the amount of oxygen in the atmosphere affects the texturing of the ZnO film.[61] Since acetonitrile is a non-oxygen containing solvent, when a 2 : 1 ratio is used, there is not enough oxygen in the reaction vessel to allow (002) growth. Instead, growth in a semipolar (103) plane is preferred rather than a non-polar one, as seen when using toluene. The conductivity of these films was very low, on the order of 10^{-4} S cm^{-1}, which is due to poor overlap of grains on the surface reducing the percolation of electrons.

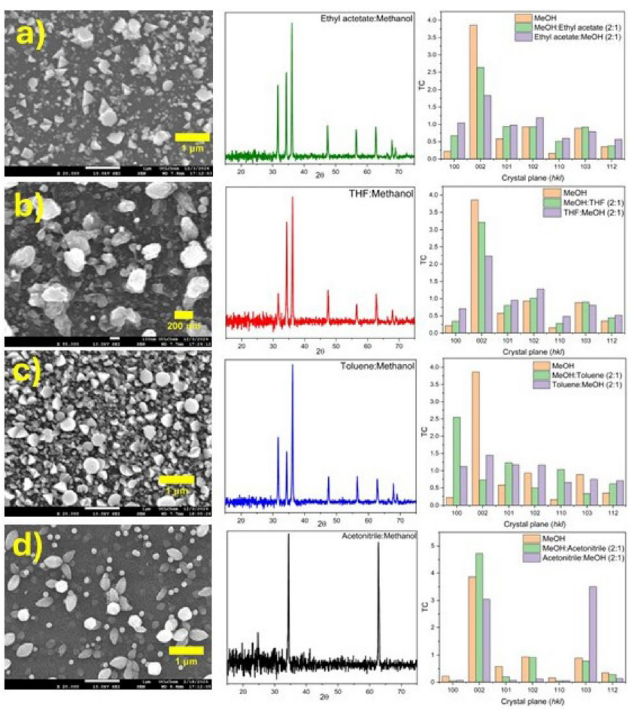

Fig. 10 SEM images of zinc oxide films using a 2 : 1 ratio of the following solvent mixtures (a) ethyl acetate:methanol, (b) THF:methanol, (c) toluene:methanol, and (d) acetonitrile:methanol. The corresponding XRD patterns are to the right of the SEM images.

Conclusions

In this study we have looked at a range of dual-solvent mixtures and their effects on zinc oxide film properties. Preferential orientation of zinc oxide crystal planes has been shown to be a direct consequence of the solvent mixture chosen. The more polar solvent mixtures cause growth to be increased along the polar *c*-axis, allowing for preferential growth in the (002) direction shown in XRD analysis.[20] Using toluene as the secondary solvent causes preferential orientation in the (001) plane with low preference for the (002) plane. These findings are significant, since the texture coefficient can be controlled using solvents of different dielectric constants, without causing any significant loss in conductivity.

WCA measurements in conjunction with XPS proved that the film morphology and surface terminations influenced the hydrophobic and hydrophilic nature of the ZnO films. Solvent mixtures containing methanol, toluene, ethyl acetate, and THF produced films that were hydrophobic, whereas hexane and acetonitrile formed films that were slightly hydrophilic in nature. These findings can be useful for antisoiling purposes for TCO devices including PV modules.

Methanol:acetonitrile films displayed the highest conductivity of 6.13 S cm^{-1} with moderate carrier mobilities. Their pyramid-like structures show the signs of some defects at the surfaces, that have separations between the grains. Annealing in air has been shown to smoothen surfaces while increasing PCE for organic solar cell design, and could further improve conductivity.[62] Methanol:hexane films showed conductivities 10 × lower than with acetonitrile but 5 × better than with just methanol. Since the solvent systems just mentioned are all highly crystalline, the use of dopants at low concentrations could form highly conductive films that can subsequently be optimised using different solvent mixtures.

The low solubility of zinc acetate in other solvents and the poor mixing between solvents can be circumvented by controlling the temperature of the solvent. In PV devices, self-texturing makes a huge difference in the PCE, where greater surface contact with fewer surface defects produces more efficient cells.[63] The ability to tune the surface morphology has the potential to produce zinc oxide films that are tailored to different photon absorbers depending on their surface morphologies.

Conflicts of interest

There are no conflicts to declare.

Data availability

The data supporting this article have been included as part of the supplementary information (SI). Supplementary information is available. See DOI: https://doi.org/10.1039/d5ma00850f.

Acknowledgements

O. R. M. would like to thank the EPSRC (grant EP/W524335/1), the DTP, UCL Chemistry and NSG (Pilkington Technology Management Limited, European Technical Centre, Hall Lane, Lathom, Nr. Ormskirk, L40 5UF, UK) for their support.

References

1 P. K. Nayak, PhD thesis, University of Oxford, 2019.
2 W. Liu, H. Li, B. Qiao, S. Zhao, Z. Xu and D. Song, *Sol. Energy*, 2022, **233**, 337–344.
3 M. A. Scarpulla, B. McCandless, A. B. Phillips, Y. Yan, M. J. Heben, C. Wolden, G. Xiong, W. K. Metzger, D. Mao, D. Krasikov, I. Sankin, S. Grover, A. Munshi, W. Sampath, J. R. Sites, A. Bothwell, D. Albin, M. O. Reese, A. Romeo, M. Nardone, R. Klie, J. M. Walls, T. Fiducia, A. Abbas and S. M. Hayes, *Sol. Energy Mater. Sol. Cells*, 2023, **255**, 112289.
4 R. Hosen, S. Sikder, M. S. Uddin, M. M. Haque, H. Mamur and M. R. A. Bhuiyan, *J. Alloys Metall. Syst.*, 2023, **4**, 100041.
5 X. Hou and K.-L. Choy, *Chem. Vap. Deposition*, 2006, **12**, 583–596.
6 P. Marchand, I. A. Hassan, I. P. Parkin and C. J. Carmalt, *Dalton Trans.*, 2013, **42**, 9406–9422.
7 D. B. Potter, I. P. Parkin and C. J. Carmalt, *RSC Adv.*, 2018, **8**, 33164–33173.
8 O. N. M. Mc Callion and M. J. Patel, *Int. J. Pharm.*, 1996, **130**, 245–249.
9 P. I. O. Filho, C. J. Carmalt, P. Angeli and E. S. Fraga, *Ind. Eng. Chem. Res.*, 2020, **59**, 1249–1260.
10 M. Tomić, I. Gràcia, E. Figueras, C. Cané and S. Vallejos, *Ceram. Int.*, 2024, **50**, 17988–18001.
11 J.-J. Max, *J. Chem. Phys.*, 2008, **128**, 224512.
12 C. Sanchez-Perez, *Mater. Adv.*, 2023, **4**, 3774–3786.
13 P. Ji, C. Wang, Z. Jiang and H. Wang, *Polym. Compos.*, 2016, **37**, 1830–1838.
14 X. Hou, F. Zhou, B. Yu and W. Liu, *Mater. Sci. Eng., A*, 2007, **452–453**, 732–736.
15 B. Ding, T. Ogawa, J. Kim, K. Fujimoto and S. Shiratori, *Thin Solid Films*, 2008, **516**, 2495–2501.
16 X. Cui, S. Mao, M. Liu, H. Yuan and Y. Du, *Langmuir*, 2008, **24**, 10771–10775.
17 P. Sharma, M. Quazi, I. R. Vazquez and N. Jackson, *J. Aerosol Sci.*, 2022, **166**, 106072.
18 National Institute of Standards and Technology (NIST), SRM 674b: Zinc Oxide, U.S. Department of Commerce, Gaithersburg, November 2017.
19 L. Xu, *Chem. Mater.*, 2009, **21**, 2875–2885.
20 A. S. Mokrushin, Y. M. Gorban, I. A. Nagornov, N. P. Simonenko, E. P. Simonenko and N. T. Kuznetsov, *Russ. J. Inorg. Chem.*, 2022, **67**, 2099–2107.
21 C. Sanchez-Perez, S. Srimuruganthan, C. Sotelo-Vazquez, S. Sathasivam, M. Wang, J. Marugán, I. P. Parkin and C. J. Carmalt, *Mater. Adv.*, 2023, **4**, 3774–3786.
22 M. Sunaina, M. Sreekanth, S. Ghosh, S. K. Mehta, A. K. Ganguli and M. Jha, *CrystEngComm*, 2017, **19**, 2264–2270.
23 S. A. Kamaruddin, K.-Y. Chan, H.-K. Yow, M. Zainizan Sahdan, H. Saim and D. Knipp, *Appl. Phys. A*, 2011, **104**, 263–268.
24 Y. O. Kosuke Takenaka and Y. Setsuhara, *Trans. Mater. Res. Soc. Jpn.*, 2012, **37**, 173–176.
25 A. H. R. Al-Sarraf, Z. T. Khodair, M. I. Manssor, R. A. A. K. Abbas and A. H. Shaban, *AIP Conf. Proc.*, 2018, **1968**, 030005.
26 L. Fanni, A. B. Aebersold, M. Morales-Masis, D. T. L. Alexander, A. Hessler-Wyser, S. Nicolay, C. Hébert and C. Ballif, *Cryst. Growth Des.*, 2015, **15**, 5886–5891.
27 S. Okeil, S. Rabet, G. Valadez Huerta, G. Raabe and G. Garnweitner, *Langmuir*, 2024, **40**, 19343–19356.
28 D. Zheng, G. Wang, W. Huang, B. Wang, W. Ke, J. L. Logsdon, H. Wang, Z. Wang, W. Zhu, J. Yu, M. R. Wasielewski, M. G. Kanatzidis, T. J. Marks and A. Facchetti, *Adv. Funct. Mater.*, 2019, **29**, 1900265.
29 S. Sánchez-Martín, S. Olaizola, E. Castaño, E. Urionabarrenetxea, G. Mandayo and I. Ayerdi, *RSC Adv.*, 2021, **11**, 18493–18499.
30 F. Li, Y. Ding, P. Gao, X. Xin and Z. L. Wang, *Angew. Chem., Int. Ed.*, 2004, **43**, 5238–5242.
31 E. Muchuweni, T. S. Sathiaraj and H. Nyakotyo, *Heliyon*, 2017, **3**, e00285.
32 S. Maroufa, *Mater. Res.*, 2016, **20**(1), 88–95.
33 G. Palasantzas and J. Barnaś, *Phys. Rev. B: Condens. Matter Mater. Phys.*, 1997, **56**, 7726–7731.
34 T. Ma, *Mater. Sci. Semicond. Process.*, 2021, **121**, 105413.
35 M. R. Waugh, G. Hyett and I. P. Parkin, *Chem. Vap. Deposition*, 2008, **14**, 366–372.
36 M. S. Hammer, D. Rauh, V. Lorrmann, C. Deibel and V. Dyakonov, *Nanotechnology*, 2008, **19**, 485701.
37 G. Wisz, I. Virt, P. Sagan, P. Potera and R. Yavorskyi, *Nanoscale Res. Lett.*, 2017, **12**, 253.
38 E. Rincon-Suarez, J. M. Mozo, A. Romero-López, S. Alcántara-Iniesta, F. J. Flores-Ruiz and L. E. Serrano, *Mater. Sci. Eng., B*, 2025, **320**, 118430.
39 P. Babelon, A. S. Dequiedt, H. Mostéfa-Sba, S. Bourgeois, P. Sibillot and M. Sacilotti, *Thin Solid Films*, 1998, **322**, 63–67.
40 M. F. Smith, S. Limwichean, M. Horprathum, J. Chaiprapa, W. W. Aye, C. Chananonnawathorn, V. Patthanasettakul, P. Eiamchai, N. Nuntawong, A. Klamchuen and P. Songsiriritthigul, *Thin Solid Films*, 2022, **751**, 139207.
41 J. G. Cuadra, A. C. Estrada, C. Oliveira, L. A. Abderrahim, S. Porcar, D. Fraga, T. Trindade, M. P. Seabra, J. Labrincha and J. B. Carda, *Ceram. Int.*, 2023, **49**, 32779–32788.
42 NSG TEC™ Product Range.

43 J. Jang, J.-H. Kim, S. Lee, C.-M. Oh, I.-W. Hwang, S. Kim, A. Park, D. Kang, C. Jang, T. Ki, H. Kim and K. Lee, *ACS Appl. Energy Mater.*, 2023, **6**, 9778–9787.
44 A. Kafizas, C. W. Dunnill and I. P. Parkin, *J. Mater. Chem.*, 2010, **20**, 8336–8349.
45 Y. Natsume and H. Sakata, *Thin Solid Films*, 2000, **372**, 30–36.
46 L. Radjehi, L. Aissani, A. Djelloul, A. Saoudi, S. Lamri, K. Nomenyo, G. Lerondel and F. Sanchette, *Metall. Mater. Eng.*, 2023, **29**, 37–51.
47 M. I. Khan, K. A. Bhatti, R. Qindeel, N. Alonizan and H. S. Althobaiti, *Results Phys.*, 2017, **7**, 651–655.
48 S. Benramache, Y. Aoun, S. Lakel and B. Benhaoua, *Mater. Res. Express*, 2019, **6**, 126418.
49 W. Lin, D. Chen, J. Zhang, Z. Lin, J. Huang, W. Li, Y. Wang and F. Huang, *Cryst. Growth Des.*, 2009, **9**, 4378–4383.
50 M. Moret, A. Abou Chaaya, M. Bechelany, P. Miele, Y. Robin and O. Briot, *Superlattices Microstruct.*, 2014, **75**, 477–484.
51 S. Nundy, A. Ghosh and T. K. Mallick, *ACS Omega*, 2020, **5**, 1033–1039.
52 H. Li, S. Yu, J. Hu and E. Liu, *Thin Solid Films*, 2018, **666**, 100–107.
53 V. Khranovskyy, T. Ekblad, R. Yakimova and L. Hultman, *Appl. Surf. Sci.*, 2012, **258**, 8146–8152.
54 R. Mardosaitė, A. Jurkevičiūtė and S. Račkauskas, *Cryst. Growth Des.*, 2021, **21**, 4765–4779.
55 G. He and K. Wang, *Appl. Surf. Sci.*, 2011, **257**, 6590–6594.
56 T. T. Chau, W. J. Bruckard, P. T. L. Koh and A. V. Nguyen, *Adv. Colloid Interface Sci.*, 2009, **150**, 106–115.
57 R. Al-Gaashani, S. Radiman, A. R. Daud, N. Tabet and Y. Al-Douri, *Ceram. Int.*, 2013, **39**, 2283–2292.
58 T. J. Frankcombe and Y. Liu, *Chem. Mater.*, 2023, **35**, 5468–5474.
59 K. Yadav, B. R. Mehta, S. Bhattacharya and J. P. Singh, *Sci. Rep.*, 2016, **6**, 35073.
60 A. E. Muslimov, A. M. Ismailov, Y. V. Grigoriev and V. M. Kanevsky, *J. Surf. Invest.: X-Ray, Synchrotron Neutron Tech.*, 2021, **15**, 1195–1199.
61 A. Taabouche, A. Bouabellou, F. Kermiche, F. Hanini, S. Menakh, Y. Bouachiba, T. Kerdja, C. Benazzouz, M. Bouafia and S. Amara, *Adv. Mater. Phys. Chem.*, 2013, **3**, 209–213.
62 A. K. Abisheva, D. A. Afanasyev, B. R. Ilyassov, A. K. Aimukhanov, V. A. Kulbachinskii and A. K. Zeinidenov, *Phys. E*, 2024, **159**, 115932.
63 M. Dkhili, G. Lucarelli, F. De Rossi, B. Taheri, K. Hammedi, H. Ezzaouia, F. Brunetti and T. M. Brown, *ACS Appl. Energy Mater.*, 2022, **5**, 4096–4107.